IN-33
180809
15P

NASA
Technical
Paper
3344

July 1993

Low-Current Traveling Wave Tube for Use in the Microwave Power Module

Raymond W. Palmer,
Peter Ramins,
Dale A. Force,
James A. Dayton,
Ben T. Ebihara,
and Robert P. Gruber

(NASA-TP-3344) LOW-CURRENT TRAVELING WAVE TUBE FOR USE IN THE MICROWAVE POWER MODULE (NASA) 15 p

N94-13110

Unclas

H1/33 0180809

NASA

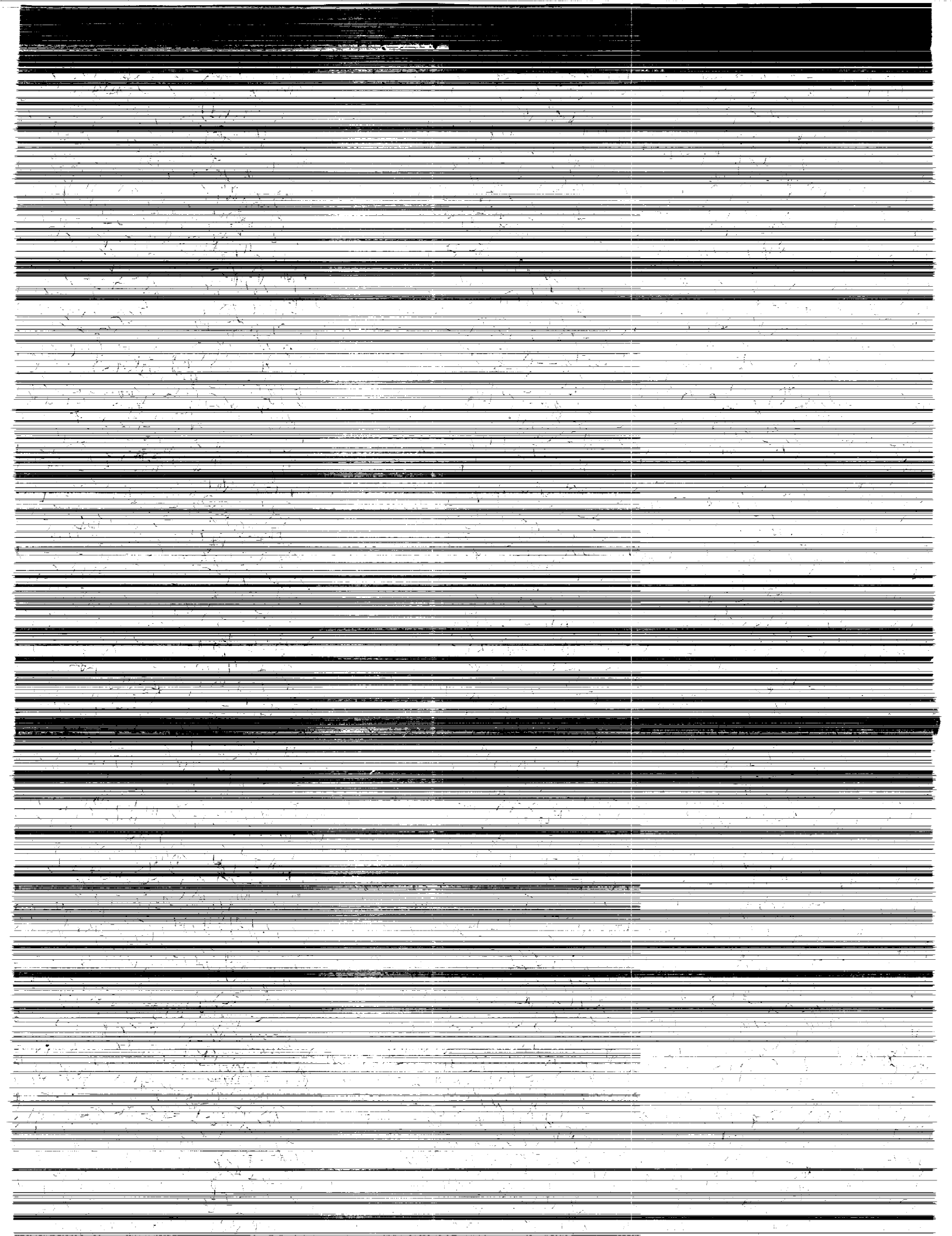

NASA Technical Paper 3344

1993

Low-Current Traveling Wave Tube for Use in the Microwave Power Module

Raymond W. Palmer,
Peter Ramins,
Dale A. Force,
James A. Dayton,
Ben T. Ebihara,
and Robert P. Gruber
Lewis Research Center
Cleveland, Ohio

National Aeronautics and Space Administration

Office of Management

Scientific and Technical Information Program

Summary

This report describes the results of a traveling-wave-tube/ multistage-depressed-collector (TWT-MDC) design study in support of the Advanced Research Projects Agency/ Department of Defense (ARPA/DOD) Microwave Power Module (MPM) Program. The study stressed the possible application of dynamic and other tapers to the rf output circuit of the MPM traveling wave tube as a means of increasing the rf and overall efficiencies and reducing the required beam current (perveance). The results indicate that a highly efficient, modified dynamic velocity taper (DVT) circuit can be designed for the broadband MPM application. The combination of reduced cathode current (lower perveance) and increased rf efficiency leads to (1) a substantially higher overall efficiency and reduction in the prime power to the MPM, and (2) substantially reduced levels of MDC and MPM heat dissipation, which simplify the cooling problems. However, the selected TWT circuit parameters need to be validated by cold test measurements on actual circuits.

Introduction

This report summarizes the results of the second stage of a NASA Lewis traveling-wave-tube/multistage-depressed-collector (TWT-MDC) design exercise in support of the Defense Advanced Research Project Agency/ Department of Defense (DARPA/DOD) Microwave Power Module (MPM) Program (refs. 1 and 2). The results of the first stage of the exercise (ref. 3) made it clear that lowering the beam current (and perveance) of the TWT would greatly ease the problems in obtaining efficient beam collection and MPM cooling, provided that the required rf output power could be maintained over the frequency range by raising the rf output efficiency of the TWT. This became the focus of the second design study, which concentrated on the evaluation of a dynamic velocity taper (DVT) and other high rf efficiency tapers for the broadband MPM traveling wave tube application.

This design study also stressed the multistage depressed collector as a key element in obtaining the required high overall TWT efficiencies in the MPM application and addressed the problem of attaining the required high overall TWT and collector efficiencies while meeting the stringent system size constraints and practical high-voltage, thermal, and mechanical design requirements. Only the interior dimensions of the collector were considered here; the electrode outer diameter of 0.3 in. will fit within an overall package one wavelength thick (0.656 in. at 18 GHz). A somewhat smaller diameter collector will be needed to fit within the program goal of a package one-half wavelength thick. However, the collector diameter needed for the one-half wavelength package will depend on the method used by the manufacturer to support and insulate the collector electrodes, which will be determined later in the program. A spent beam refocuser (SBR) with controlled beam expansion, a key element in obtaining adequately high MDC efficiencies, was added because of the particular combination of size constraints, and cooling and high-voltage standoff requirements.

This report describes the procedure for the tapered circuit TWT design and gives the results of analyses from several computer models across the entire bandwidth.

Selected Symbols

a	mean helix radius, in.
$\bar{E}$	average disk energy, eV
$E_{\min}$	energy of slowest disk, eV
K_a	Pierce interaction impedance at the mean helix radius, Ω
K_p	Pierce interaction impedance integrated over the beam, Ω
$\bar{r}$	average disk radius, in.
V_0	cathode voltage, V
η_{rf}	rf efficiency

TWT Slow Wave Circuit Description and Performance Results

The first task in the baseline design process was to acquire input parameters that characterize the TWT across the entire bandwidth. Chief among these are the helix phase velocity and the interaction impedance. To obtain these parameters, we assumed a vaned structure and analyzed it according to the prescription of reference 4. Our assumed geometry and the results of the study are shown in figure 1.

The other parameters used in the baseline design are shown in table I. Note that the current is 125 mA, a reduction of more than 28 percent from our previous MPM study (ref. 3). The helix lengths were determined by requiring that at the lower band edge (1) there be sufficient gain to develop a bunched beam by the start of the sever, (2) the sever/attenuator length result in an efficient restart of the signal, and (3) the overall length produce saturation with an input power of 30 dBm. The peak magnetic field is $\sqrt{2}$ times the Brillouin field necessary to contain the beam. (The model demands a smaller value of field than a practical, or "real" TWT, since it cannot simulate the complex radial and thermal effects of an actual beam.) The attenuation was assumed to vary linearly across the bandwidth, from 0.8 dB/in. at 6 GHz to 1.6 dB/in. at 18 GHz. The rest of the parameters were the same as those used in reference 3.

The baseline parameters were used in Lewis Research Center's revised Detweiler large-signal code (ref. 5). Saturated

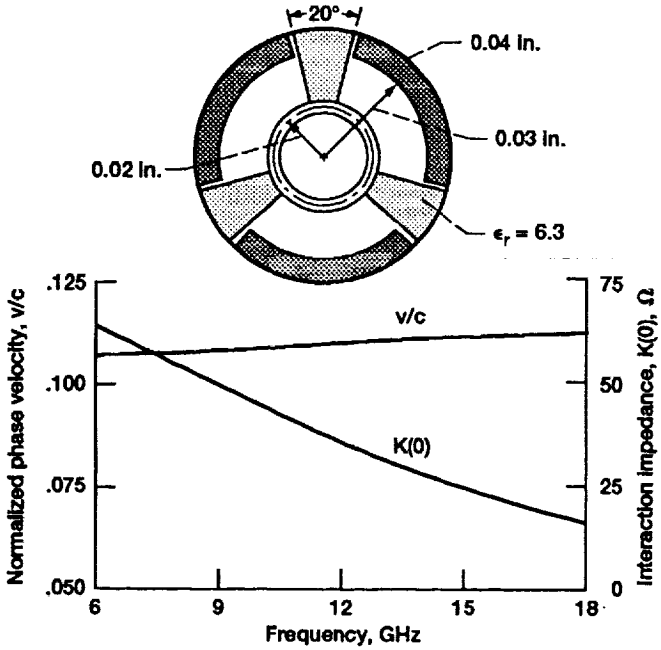

Figure 1.—Normalized phase velocity and centerline interaction impedance as calculated from reference 4. Geometry shown in inset. (Helix pitch, 0.0209 in.$^{-1}$; c, speed of light; ϵ_r, relative permittivity.)

TABLE I.—INPUT PARAMETERS FOR THE BASELINE DESIGN

Frequency, GHz	6 to 18
Average helix radius, in.	0.02
Electron beam radius, in.	0.008
Cathode voltage, kV	3.5
Beam current, mA	125
Centerline interaction impedance	See figure 1
Normalized helix phase velocity, *v/c*	See figure 1
Centerline peak magnetic flux density, T	0.2657
Period of periodic permanent magnet (PPM) stack, in.	0.2169
Length of input helix, in.	0.60
Length of attenuator/sever section, in.	0.30
Length of output helix, in.	2.10

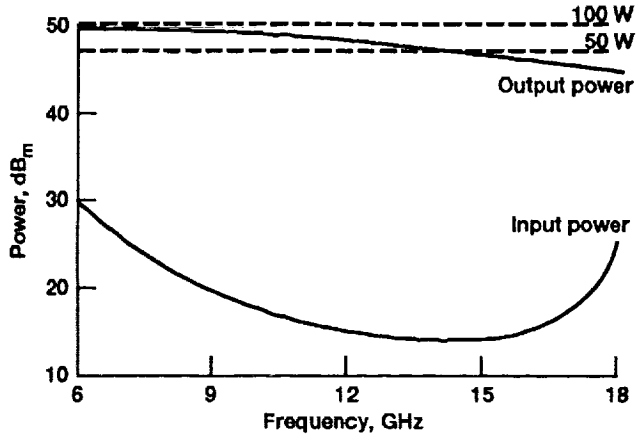

Figure 2.—Saturation input and output power for baseline design across the bandwidth.

TABLE II.–SATURATED PERFORMANCE FOR BASELINE, DVT, AND DVT+ DESIGNS

(a) Baseline

	Frequency, GHz				
	6	9	12	15	18
RF efficiency, percent	20.9	19.3	15.4	10.4	7.2
Gain, dB	19.5	29.1	32.3	31.5	18.9

(b) DVT

	Frequency, GHz				
	6	9	12	[a]15	18
RF efficiency, percent	22.0	22.1	18.7	14.7	9.1
Gain, dB	19.8	29.8	33.1	33.1	20.0

(c) DVT+

	Frequency, GHz				
	6	9	12	[a]15	18
RF efficiency, percent	24.7	24.2	20.1	17.2	12.5
Gain, dB	19.4	31.2	35.4	32.7	23.4

[a]DVT design optimized at this frequency.

output power and rf input power, both in dBm, are shown as functions of frequency in figure 2, and efficiency and gain are listed in table II(a). The bowl-shaped drive relationship in figure 2 is typical of all the studies that were performed and suggests that tailoring the output of the solid-state driver for overall gain equalization could be a significant task.

To meet the power requirements of the MPM program, we then designed a dynamic velocity taper (DVT) for operation at 15 GHz. We felt that the resultant increase in efficiency might reverse the sag in the output power curve, but perhaps at the expense of reduced power at the lower frequencies.

The DVT was designed according to reference 6, wherein the Pierce velocity parameter (ref. 7) is prescribed by

$$b = b_0 + \alpha\left(\frac{K_a}{K_p}\right)^{1/3}\left[exp\left(\tau_z\left(z - z_0\right)\right) - 1\right]$$

with resultant phase velocity variation

$$\frac{v}{v_0} = \frac{1 + b_0 C}{1 + bC}$$

Here K_a is the Pierce interaction impedance at the mean helix radius, K_p is the Pierce interaction impedance integrated over the beam, b is the Pierce velocity parameter, v is the phase velocity, C is the Pierce interaction parameter (ref. 7), and z is the axial distance along the circuit. The zero subscript refers to quantities at the start of the taper. The cube root of the impedance ratio is reported at the taper start in the large-signal program. The parameter τ_z is given by the slope of a line segment tangent to the curve of ln η_{rf} at saturation as a function of axial distance z. The line segment starts at some taper start z_0 chosen to maximize rf efficiency. The parameter α is also determined so as to maximize rf efficiency. The procedure for determining τ_z is illustrated in figure 3.

Best performance occurred with z_0 = 2 in., τ_z = 4.4 in.$^{-1}$, and α = 0.03. These taper parameters resulted in a nonlinear reduction in phase velocity over the last inch of output helix of 17 percent to 16 percent across the 6- to 18-GHz bandwidth. Efficiency and gain produced by the large-signal code are shown in table II(b). Note by comparison with table II(a) the desirable result of significantly increased performance across the entire bandwidth. In particular, at 15 GHz, the design frequency, output power increased by more than 41 percent. The favorable results at all frequencies suggest that large values of drive provide adequate bunching of the beam so that the DVT can operate efficiently over a wide band of frequencies.

Recent TWT design experience in a 32-GHz development program at Lewis (ref. 8) suggested that we try one further performance-enhancing technique. As we did in that program, we added a short section of constant pitch to the end of the DVT. Over its length the extended section continued the pitch at the end of the DVT. These two sections, considered as a unit, we call the DVT+.

Optimum performance occurred at 15 GHz, the original DVT design frequency, when the constant-pitch section was made 0.15 in. long. Output power that results from the extension is shown in figure 4 across the band and compared with the baseline and DVT cases. This figure shows the dramatic improvement gained in the evolution of the design concepts. Table II(c) gives rf efficiency and gain over the band and can be compared directly with the DVT results of table II(b). Note that further improvement results throughout the entire bandwidth, and even the radar MPM requirements are very nearly met. At 15 GHz, the DVT+ caused output power to increase by 17 percent over the DVT result; this

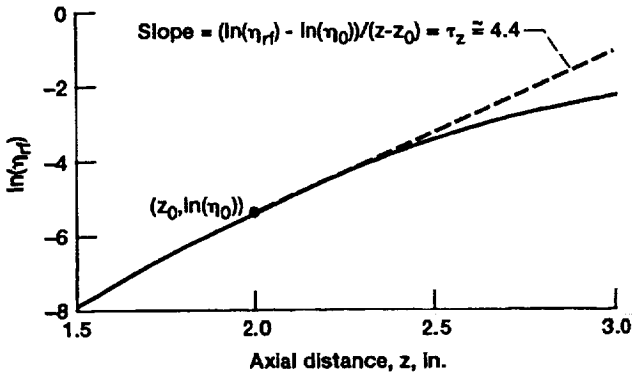

Figure 3.—Plot of ln(η_{rf}) as a function of axial distance, operating at saturation at 15 GHz. Slope determines τ_z for the design of the DVT. (Start value = z_0 = 2.0 in.)

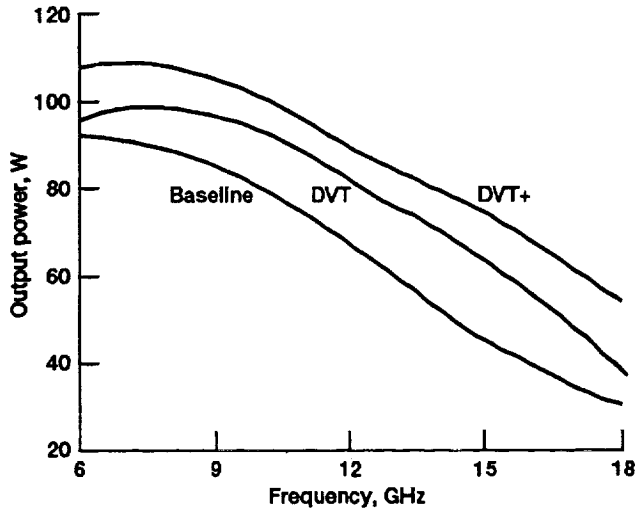

Figure 4.—Output power across the bandwidth for baseline, DVT, and DVT+ designs.

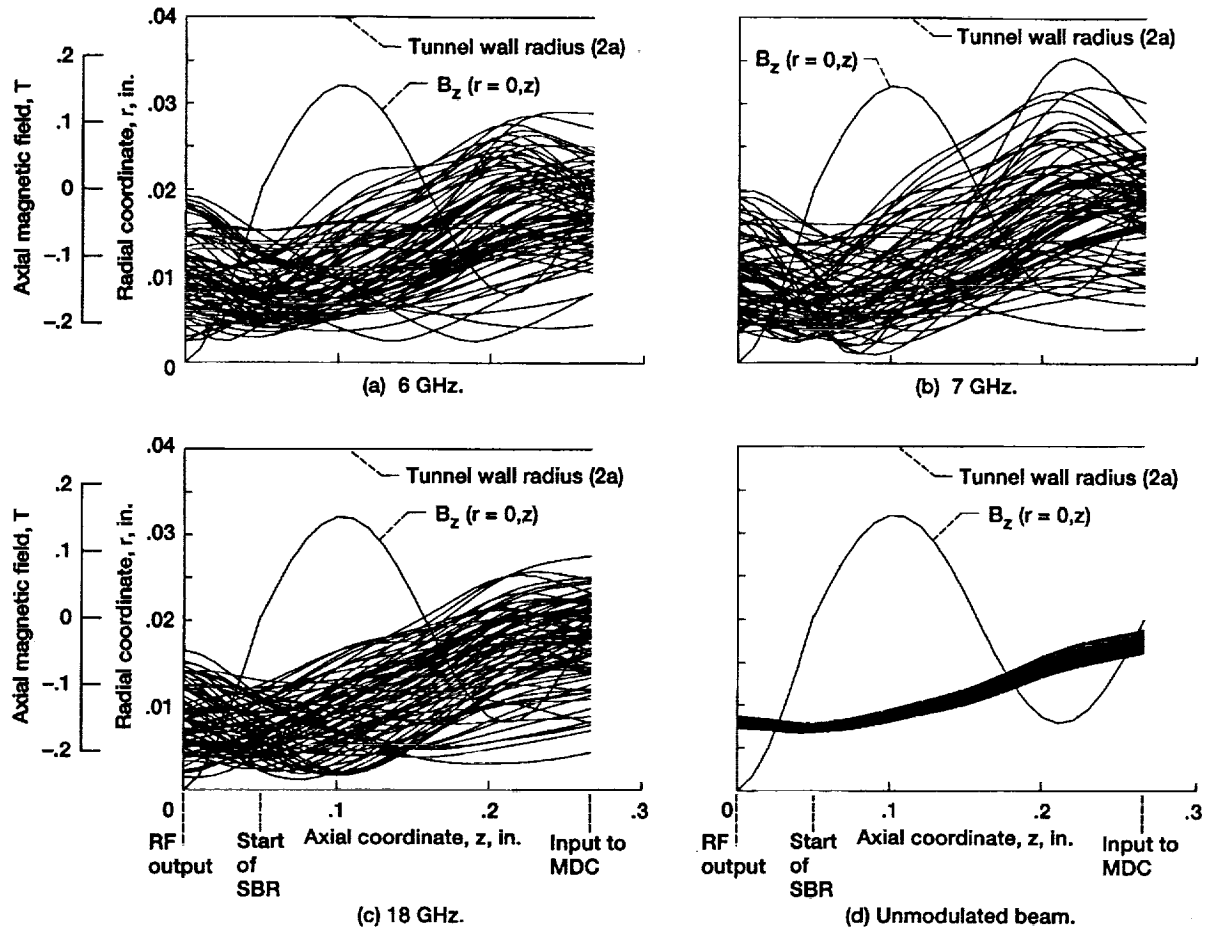

Figure 5.—Disk outer radii trajectories and axial magnetic field in spent beam refocuser (SBR) for TWT operating at saturation at various frequencies. Focusing field in SBR reduced to 60 percent of TWT magnetic field.

represents an increase of nearly 65 percent over the baseline result. Small adjustments in parameters such as cathode voltage or beam current could possibly allow the tailoring of output power to rigorous requirements over the frequency range.

MDC and Spent Beam Refocuser (SBR) Models and Design Constraints

The SBR was modeled with the revised Detweiler TWT computer code so that the effects of beam debunching and controlled expansion could be analyzed simultaneously. We felt that some controlled beam expansion was mandatory to (1) reduce the amount of kinetic power associated with radial motion caused by space-charge-driven beam expansion when the focusing field is removed (power which cannot be recovered in the MDC), and (2) to make possible the design of an MDC sufficiently long (z-direction) to provide realistic high-voltage standoff and cooling.

The scope of the SBR investigation, however, was quite limited: only SBR's consisting of two or three additional magnets of reduced but uniform strength, in a continuation of the periodic permanent magnet (PPM) stack past the rf output, were considered. SBR field strengths in the range of 0.5 to 0.7 of that of the TWT PPM stack were investigated.

MDC performance was modeled with the Herrmansfeldt electron trajectory computer program (ref. 9). The MDC design was produced by iterative performance analyses at the following three TWT operating frequencies: the frequency producing maximum η_{rf} (7 GHz) and the band-edge frequencies (6 and 18 GHz). Normally, maximum η_{rf} occurs near midband. In the present case, however, because of the 100 W requirement for the 7- to 11-GHz radar band and the peculiarities of the DVT+ design, maximum η_{rf} occurred very near the lower band edge. The MDC design was largely optimized at 7 GHz since the TWT output at 6 GHz (108 W) greatly exceeds the electronic countermeasures (ECM)

TABLE III. – SUMMARY OF SPENT BEAM CHARACTERISTICS AT END OF REFOCUSER (INPUT TO MDC). TWT OPERATING AT SATURATION AT VARIOUS FREQUENCIES

(a) Range of disk edge angles

Frequency, GHz	Without beam expansion[a]	With beam expansion[b]
	Disk edge angle, deg	
6	-14.4 to 8.3	-8.8 to 5.8
7	-21.9 to 10.2	-11.2 to 6.0
18	-6.7 to 10.2	-4.3 to 5.9

(b) Average disk edge angle and standard deviation

Frequency, GHz	Without beam expansion[a]		With beam expansion[b]	
	Average angle, deg	Standard deviation	Average angle, deg	Standard deviation
6	0.54	4.8	0.20	3.4
7	0	5.3	.22	4.0
18	.38	4.1	1.3	2.4

(c) Disk edge radii (normalized to average helix radius a)

Frequency, GHz	Without beam expansion[a]		With beam expansion[b]	
	Average radius, $\bar{r}/a$	Maximum radius (beam edge), r_{max}/a	Average radius, $\bar{r}/a$	Maximum radius (beam edge), r_{max}/a
6	0.41	0.70	0.90	1.44
7	.41	.76	.91	1.51
18	.40	.73	.88	1.38

[a]Spent beam drifts past rf output in a continuation of the PPM stack with two additional full-strength magnets.

[b]Spent beam drifts past rf output in a continuation of the PPM stack with two additional 60 percent strength magnets.

requirement and might well be reduced by a circuit design change or by controlling the rf input drive.

The secondary-electron-emission (SEE) losses in the MDC were modeled by injecting secondaries with kinetic energy of 10 eV from the points of impact of the primary charges on the electrode surfaces back along the angle of incidence (ref. 10). A SEE yield of 0.5 was assumed. The effects of energetic secondaries were ignored. The MDC was designed with low-SEE-yield electrode surfaces (isotropic graphite) in mind. An optimized high-SEE-yield (copper) electrode MDC would have its own (different) electrode shapes and operating potentials.

An MDC active inner diameter of 0.30 in. was selected somewhat arbitrarily as a compromise in an attempt to minimize the loss in MDC efficiency (with decreasing MDC radial size) while providing considerable latitude for the high-voltage, thermal, and mechanical designs. Within this size constraint the axial length of the MDC was made as large as possible without significantly compromising the collector efficiency. The four-stage collector design was optimized for operation of the TWT at saturation and does not provide a highly depressed (>0.85V_0) electrode to minimize dissipated power and power density for the case of zero rf input power. However, the depression was increased from 0.75V_0 in reference 3 to nearly 0.8V_0. This combined with the reduced beam current (125 versus 175 mA) would bring the collector dissipation down to the level of that for saturated operation and make the fifth stage proposed in reference 3 unnecessary.

Spent Beam Refocuser Design and Performance

The SBR design and charge trajectories for 6, 7, and 18 GHz, and the unmodulated (dc) beams are shown in figures 5(a) to 5(d), respectively. Performance is summarized in table III. The 0.22-in.-long SBR consists of two 60-percent-strength PPM stack magnets. Compared to the same beam (at the SBR input) drifting in a full-strength continuation of the PPM stack, it can be seen that the SBR significantly reduces the range and the standard deviation of the disk edge angles at the MDC input, and provides a beam (area) expansion of a factor of nearly 5 (based on $\bar{r}$).

The SBR also provides for conversion of some space-charge potential energy into axial kinetic energy. This is illustrated in figure 6 and table IV. Both $\bar{E}$ and E_{min} are increased substantially in all cases. Without controlled beam expansion, some of the potential energy of the beam space charge would become irrecoverable kinetic energy associated with radial velocity components of the charges. The spent beam energy distributions at the input to the MDC are shown in figure 7. The debunching action is almost complete after drift through $1\frac{1}{4}$ magnetic periods past the rf output (two magnets), with only relatively small changes in the energy distribution occurring after that.

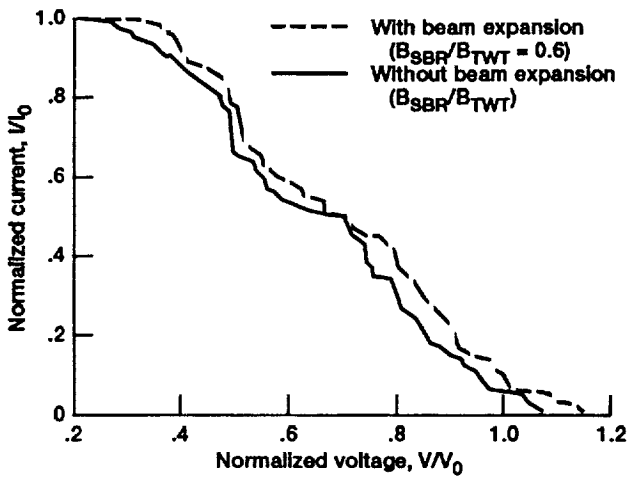

Figure 6.—Computed spent-beam energy at MDC input for TWT operation at saturation at 7 GHz showing recovery in spent beam refocuser.

TABLE IV.– DEMONSTRATION OF ENERGY RECOVERY IN SPENT BEAM REFOCUSER. TWT OPERATING AT SATURATION AT VARIOUS FREQUENCIES (RESULTS AT END OF SBR)

Frequency, GHz	Without beam expansion[a]		With beam expansion[b]	
	E_{min}, eV	$\bar{E}$, eV	E_{min}, eV	$\bar{E}$, eV
6	882	2311	1258	2485
7	890	2380	1185	2485
18	1478	2728	1712	2911

[a]Spent beam drifts past rf output in a continuation of the PPM stack with two additional full-strength magnets.

[b]Spent beam drifts past rf output in a continuation of the PPM stack with two additional 60 percent strength magnets.

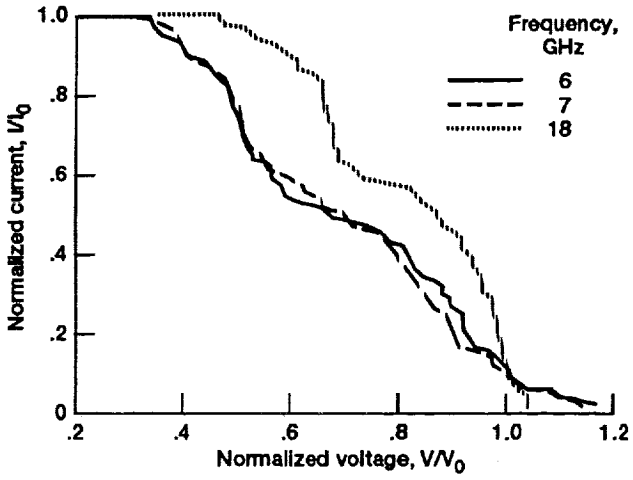

Figure 7.—Computed spent-beam energy at MDC input for TWT operation at saturation at 6, 7, and 18 GHz.

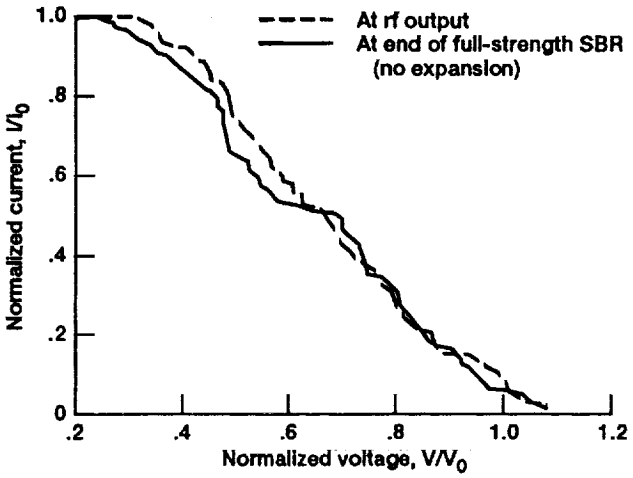

Figure 8.—Computed spent-beam energy at rf output and end of full-strength spent beam refocuser showing effect of debunching. TWT operating at saturation at 7 GHz.

The effect of debunching on the spent beam energy distribution in the absence of controlled beam expansion is illustrated in figure 8 for the case of 7 GHz. The effect of debunching without expansion is quite undesirable, with E_{min} being reduced from $0.33V_0$ to $0.25V_0$. A part of this reduction in kinetic energy is due to beam compression as it drifts in a continuation of the PPM stack (from $\bar{r}=0.49a$ to $\bar{r}=0.41a$ in this case). The results at 6 and 18 GHz were quite similar.

MDC Design and Performance

The four-stage, axisymmetric MDC geometry, the applied potentials, the equipotential lines, and the charge trajectories are shown in figures 9 to 12 for the saturated rf and unmodulated (DC) beams. The corresponding TWT-SBR-MDC power distributions, electrode dissipation, current distributions, and efficiencies are shown in tables V to VIII. For convenience each corresponding figure-table pair is shown on a separate page. The overall TWT efficiency includes a heater power of 3 W, but uses an overly optimistic (zero helix current) calculation of electron beam interception. A more realistic estimate of the interception is given later in this section. The electrode geometry was designed to maximize beam collection on or near the MDC sidewalls in order to provide a short heat conduction path outward for the dissipated (thermal) power.

The somewhat low MDC efficiencies are due to the large velocity spread in the beam and somewhat reduced sorting efficiency (refs. 11 and 12) caused by the high space-charge forces in the spent beam, which lead to significant irrecoverable energy associated with radial motion. At 6GHz, significant efficiency is lost because of backstreaming current caused by the particularly undesirable combination of large negative angles at fairly large radii and low energy for two of the disks at the MDC input. This could be reduced or eliminated by fine tuning the SBR. At 18 GHz the collector efficiency is limited by the low values of collector depression required for the high η_{rf} operating points at 6 and 7 GHz. The required prime power at 18 GHz, however, is well below that at 6 or 7 GHz in spite of the low overall efficiency.

In general, the collector efficiencies are comparable to those in reference 3. The benefits of reduced perveance (0.6 μP versus 0.85 μP) are offset by the substantially higher η_{rf}'s obtained with the DVT+ circuit. The all-important overall efficiency, however, significantly exceeds even the TWT/five-stage collector performance in reference 3. The overall efficiencies are overestimated because the computer model gives zero or near-zero beam interception. With a more realistic beam interception of $0.02V_0I_0$, the overall efficiency would be 51.1, 53.2, and 33.0 percent at 6, 7, and 18 GHz, respectively. These results suggest that with the DVT+ TWT circuit design, the goal of 50 percent overall efficiency at and

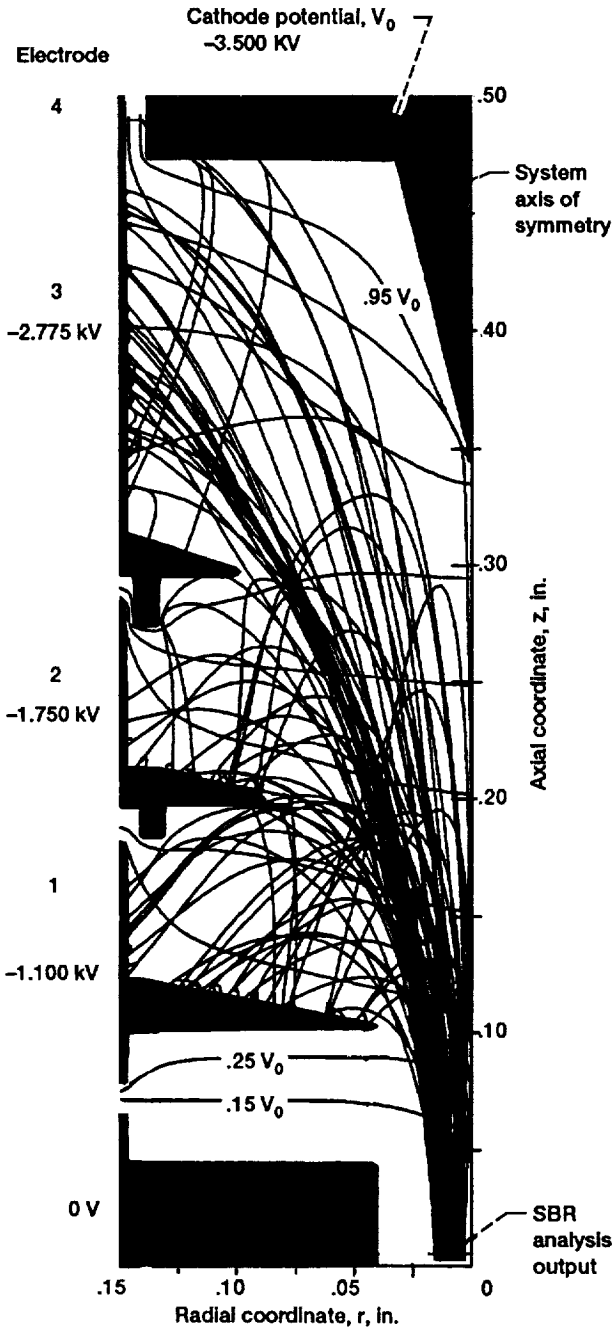

Figure 9.—Charge trajectories in four-stage depressed collector with TWT operating at saturation at 7 GHz. (Active MDC size, 0.30 in. i.d. by 0.43 in. high.)

TABLE V.—COMPUTED PERFORMANCE OF TWT AND FOUR-STAGE DEPRESSED COLLECTOR AT SATURATION AT 7 GHz

[Computed trajectories shown in fig. 9.]

(a) TWT-SBR-MDC performance[a]

Electrode (fig. 9)	Voltage (with respect to ground), kV	Current, mA	Recovered power, W	Dissipated power, W
Polepiece	0	0	0	0
1	-1.100	40.4	44.4	25.5
2	-1.750	34.3	60.0	20.8
3	-2.775	47.7	132.2	23.3
4	-3.500	2.3	8.2	2.0
Totals		124.7	244.9	71.5

(b) Computed efficiency

System component	Efficiency, percent
Collector	77.4
Overall	55.4

(c) Power balance in TWT-SBR-MDC system

Component of power	Power, W
Beam interception	0.8
Total rf conversion	[b]121.6
Recovered power	244.9
MDC dissipation	71.5

[a]Assumes an isotropic-graphite electrode secondary-electron-emission yield of 0.5.

[b]Includes output power of 109.1 W, assumed window losses of 0 W, and circuit losses of 12.5 W.

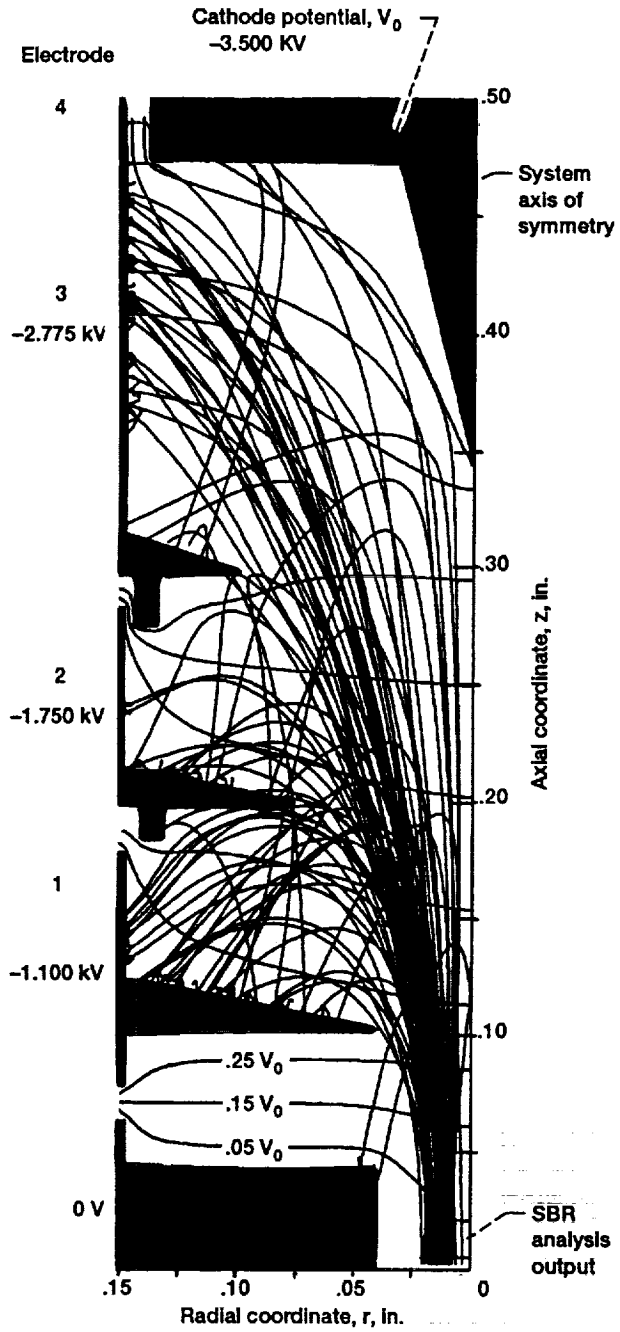

Figure 10.—Charge trajectories in four-stage depressed collector with TWT operating at saturation at 6 GHz. (Active size, 0.30 in. i.d. by 0.43 in. high.)

TABLE VI.—COMPUTED PERFORMANCE OF TWT AND FOUR-STAGE DEPRESSED COLLECTOR AT SATURATION AT 6 GHz

[Computed trajectories shown in fig. 10.]

(a) TWT-SBR-MDC performance[a]

Electrode (fig. 10)	Voltage (with respect to ground), kV	Current, mA	Recovered power, W	Dissipated power, W
Polepiece	0	3.1	0	4.4
1	-1.100	43.0	47.3	26.7
2	-1.750	28.9	50.6	19.2
3	-2.775	47.7	132.2	27.0
4	-3.500	2.3	8.2	2.6
Totals		125.0	238.3	79.9

(b) Computed efficiency

System component	Efficiency, percent
Collector	74.9
Overall	53.2

(c) Power balance in TWT-SBR-MDC system

Component of power	Power, W
Beam interception	0
Total rf conversion	[b]121.1
Recovered power	238.3
MDC dissipation	79.9

[a]Assumes an isotropic-graphite electrode secondary-electron-emission yield of 0.5.

[b]Includes output power of 108.1 W, assumed window losses of 0 W, and circuit losses of 13.0 W.

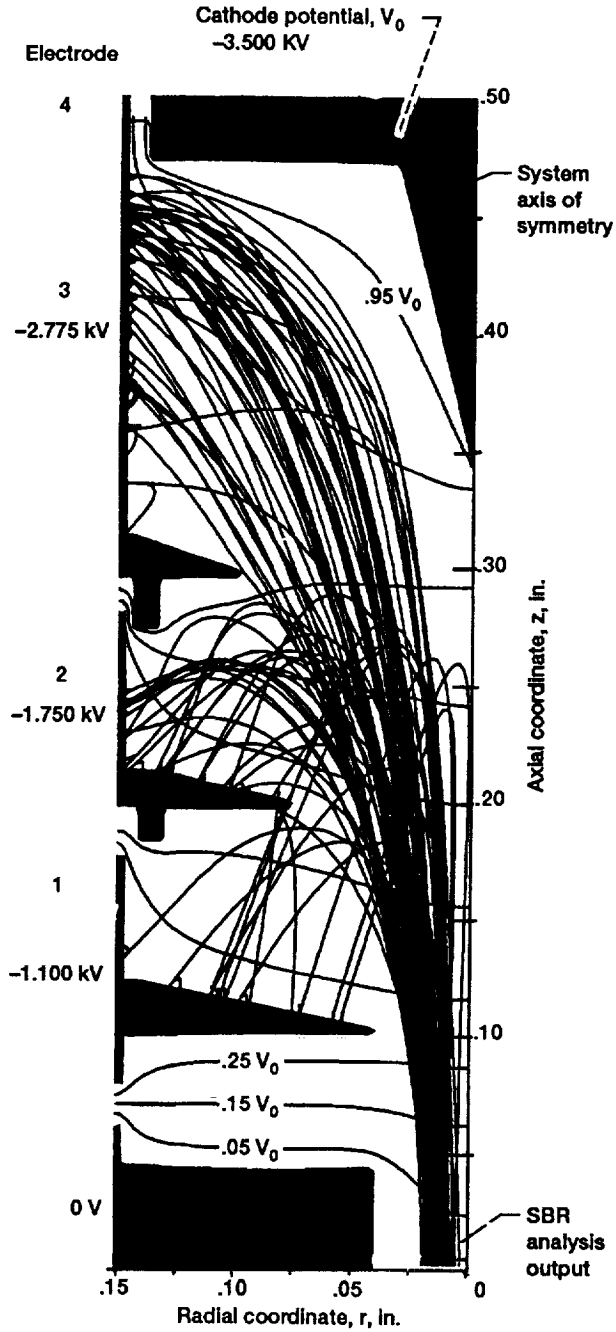

Figure 11.—Charge trajectories in four-stage depressed collector with TWT operating at saturation at 18 GHz. (Active MDC size, 0.30 in. i.d. by 0.43 in. high.)

TABLE VII.—COMPUTED PERFORMANCE OF TWT AND FOUR-STAGE DEPRESSED COLLECTOR AT SATURATION AT 18 GHz

[Computed trajectories shown in fig. 11.]

(a) TWT-SBR-MDC performance[a]

Electrode (fig. 11)	Voltage (with respect to ground), kV	Current, mA	Recovered power, W	Dissipated power, W
Polepiece	0	0	0	0
1	-1.100	13.3	14.6	13.4
2	-1.750	39.8	69.7	27.6
3	-2.775	71.9	199.4	47.6
4	-3.500	0	0	0
Totals		125.0	283.8	88.7

(b) Computed efficiency

System component	Efficiency, percent
Collector	76.2
Overall	34.8

(c) Power balance in TWT-SBR-MDC system

Component of power	Power, W
Beam interception	0
Total rf conversion	[b] 65.6
Recovered power	283.8
MDC dissipation	88.7

[a]Assumes an isotropic-graphite electrode secondary-electron-emission yield of 0.5.

[b]Includes output power of 54.7 W, assumed window losses of 0 W, and circuit losses of 10.9 W.

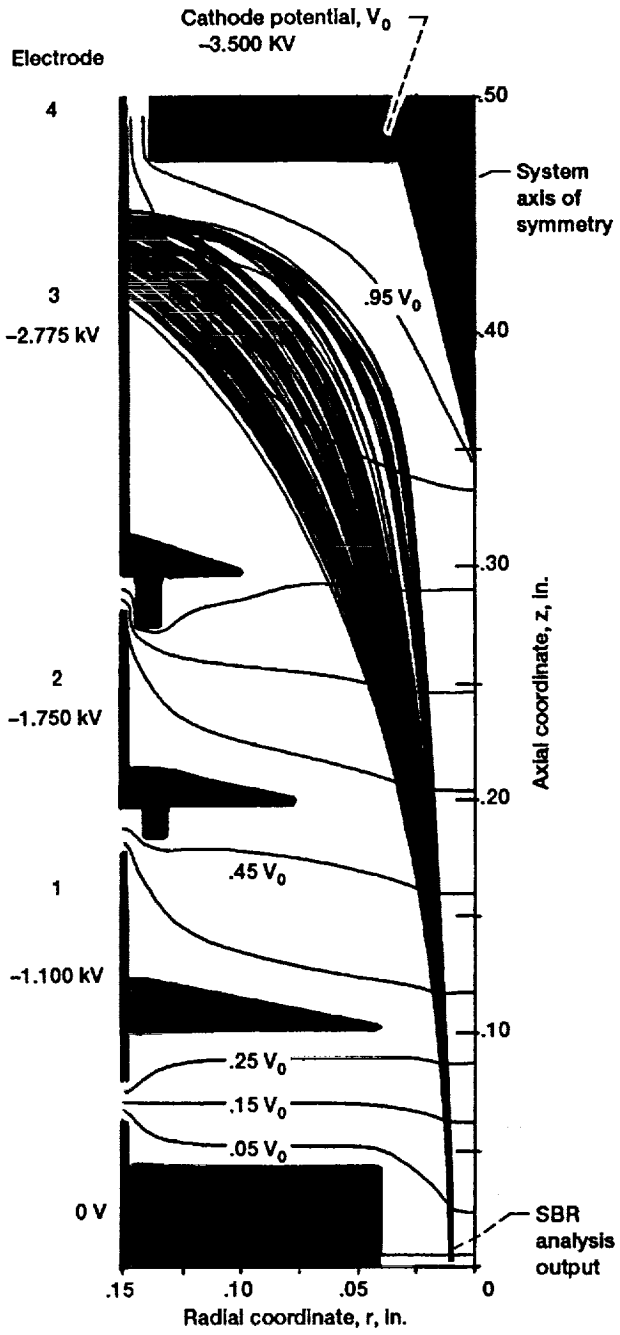

Figure 12.—Charge trajectories in four-stage depressed collector with TWT operating with unmodulated (dc) beam. (Active MDC size, 0.30 in. i.d. by 0.43 in. high.)

TABLE VIII.—COMPUTED PERFORMANCE OF TWT AND FOUR-STAGE DEPRESSED COLLECTOR WITH UNMODULATED (dc) BEAM

[Computed trajectories shown in fig. 12.]

(a) TWT-SBR-MDC performance[a]

Electrode (fig. 12)	Voltage (with respect to ground), kV	Current, mA	Recovered power, W	Dissipated power, W
Polepiece	0	0	0	0
1	-1.100	0	0	0
2	-1.750	0	0	0
3	-2.775	125.0	346.9	90.7
4	-3.500	0	0	0
Totals		125.0	346.9	90.7

(b) Computed efficiency

System component	Efficiency, percent
Collector	79.3
Overall	---

(c) Power balance in TWT-SBR-MDC system

Component of power	Power, W
Beam interception	0
Total rf conversion	----
Recovered power	346.9
MDC dissipation	90.7

[a]Assumes an isotropic-graphite electrode secondary-electron-emission yield of 0.5.

TABLE IX. – SUMMARY OF NASA ESTIMATES OF MICROWAVE POWER MODULE SYSTEM PERFORMANCE FOR TWT WITH DVT+ AND FOUR-STAGE DEPRESSED COLLECTOR

	DVT+ helix	
	Saturation at 7 GHz	Unmodulated (dc) beam
Beam voltage, kV	3.5	3.5
Beam current, mA	125	125
rf output, W	109	0
rf losses, W	12.5	0
Beam interception, W	9	4.5
Heater power, W	3	3
Collector dissipation, W	72	91
Solid state driver input, W	11	10
Electronic power conditioning (EPC) losses, W	24	11
TWT efficiency, percent	53	0
Microwave power module (MPM) efficiency, percent	45.2	0
Total dissipation, W	132	120
Total power in, W	241	120

near the maximum-prime-power operating point appears to be readily achievable even with a four-stage collector.

The goal that the MDC might be made longer to ease heat transfer and high-voltage standoff difficulties with the reduced beam current was not realized. The expected beneficial effect of reduced space charge in the beam was partially offset by lower spent beam electron velocities due to the higher η_{rf}. The thermal MDC dissipation, however, has been substantially reduced compared to the four-stage collector in reference 3, thus simplifying the MDC cooling problem.

The computed secondary-electron-emission losses for the worst case (6 GHz) reduced the MDC efficiency from 76.7 to 74.9 percent. For the best case (18 GHz) the losses were negligible. These losses were significantly smaller than those in reference 3, possibly because of smaller injection angles and reduced space-charge-driven beam expansion. However, as mentioned previously, the effects of energetic secondary electrons were ignored entirely. Based on past experience (ref. 13), a 10- to 12-percent (not percentage point) degradation in the overall efficiency might be expected by using machined copper instead of machined isotropic graphite MDC electrode surfaces (eg., 49 percent instead of 55 percent at 7 GHz). A preliminary look at the high-voltage, mechanical, and thermal designs indicates that it should be possible to incorporate these MDC designs in a practical MPM TWT. However, the packaged MDC could have a considerably larger axial dimension than the 0.43-in. active length.

MPM Performance

A summary of the estimated MPM performance is presented in table IX. An electronic-power-conditioning efficiency of 90 percent was assumed. The maximum prime power to the MPM was 241 W, a significant reduction from the 317 W estimated in reference 3.

Concluding Remarks

Application of the DVT and DVT+ concepts to the MPM traveling wave tube were investigated. The combination of reduced cathode current and increased rf efficiency lead to the following:

1. Substantially higher overall efficiency and reduction in the prime power to the TWT
2. Substantially reduced levels of MDC dissipation, which ease the cooling problem
3. Reduced PPM stack focusing requirements and increased margin for stability

The results appear to be very promising. However, the validity of the TWT parameters used (notably, the phase velocity and impedance as functions of frequency) needs to be verified by cold test measurements on actual or scaled DVT+ circuits.

This initial design study was aimed at a first-generation MPM which need not fit within a one-half-wavelength-thick package. The results suggest that an efficient MDC, using conventional, high-voltage standoff, thermal, and mechanical design and fabrication techniques, can be designed for the MPM TWT. The overall TWT efficiency goal of 50 percent for radar applications appears to be readily achievable. A preliminary look at MDC fabrication and possible electronic-power-conditioning approaches indicates that the fairly large number of collector stages considered in this study (i.e., four) does not represent a significant complication. The improved efficiency, compared to two and three stages, leads to substantially lower prime power requirements and simplifies the cooling problem. The substantial secondary-electron-emission losses in the MDC indicate that the use of isotropic graphite MDC electrodes is highly desirable. This design study was fairly limited in scope. Some performance improvements should be possible by fine tuning the TWT, SBR, and MDC designs.

Lewis Research Center
National Aeronautics and Space Administration
Cleveland, Ohio, November 2, 1992

References

1. Microwave Power Module Design Study. Final Report. Hughes Aircraft Co. and Naval Research Laboratories, Contract N00014-90-C-2318 CDRLA002, Washington, DC, Apr. 1992.

2. Microwave Power Module Study (Electronic Warfare). Teledyne MEC and Naval Research Laboratories, Contract N00014–90–C–2298, Washington, DC, Apr. 1992.

3. Ramins, P., et al.: Interim Report on the Analysis of the Microwave Power Module. NASA TM–106012, May 1992.

4. Paik, S. F.: Design Formulas for Helix Dispersion Shaping. IEEE Trans. Electron Devices, vol. ED–16, no. 12, Dec. 1969, pp. 1010-1014.

5. Detweiler, H. K.: Characteristics of Magnetically Focused Large-Signal Traveling-Wave Amplifier. Technical Report No. RADC–TR–68–433, Oct. 1968.

6. Kosmahl, H. G.; and Peterson, J. C.: A TWT Amplifier With a Linear Power Characteristic and Improved Efficiency. NASA TM–83477, 1984. (Also, AIAA Pager 84–0762, 9184.)

7. Gewartowski, J. W.; and Watson, H. A.: Principles of Electron Tubes, Including Grid-Controlled Tubes, Microwave Tubes, and Gas Tubes. D. Van Nostrand Company Inc., Princeton, NJ, 1965.

8. Curren, A. N., et al.: A Low-Power, High-Efficiency Ka-Band TWTA. IEDM Technical Digest: International Electron Devices Meeting, 1991, IEEE, New York, 1991, pp. 581–583.

9. Herrmannsfeldt, W. B.: Electron Trajectory Program - SLAC Computer Program. Report SLAC–166, Stanford Linear Accelerator Center, CA, 1979.

10. Force, D.A.: Calculation of Secondary Electron Trajectories in Multistage Depressed Collectors for Microwave Amplifiers. NASA TP–2664, 1986.

11. Kosmahl, H. G.: Modern Multistage Depressed Collectors - A Review. Proc. IEEE, vol. 70, Nov. 1982, pp. 1325–1334.

12. Kosmahl, H. G.: How to Quickly Predict the Overall TWT and the Multistage Depressed Collector Efficiency. IEEE Trans. Electron Devices, vol. ED–27, Mar. 1980, pp. 526–529.

13. Ramins, P; and Ebihara,B.T.: Improvements in MDC and TWT Overall Efficiency Through the Application of Carbon Electrode Surfaces - Multistage Depressed Collectors. IEEE Trans. Electron Devices, vol. ED–35, Nov. 1986, pp.1915–1924.

REPORT DOCUMENTATION PAGE

Form Approved
OMB No. 0704-0188

Public reporting burden for this collection of information is estimated to average 1 hour per response, including the time for reviewing instructions, searching existing data sources, gathering and maintaining the data needed, and completing and reviewing the collection of information. Send comments regarding this burden estimate or any other aspect of this collection of information, including suggestions for reducing this burden, to Washington Headquarters Services, Directorate for information Operations and Reports, 1215 Jefferson Davis Highway, Suite 1204, Arlington, VA 22202-4302, and to the Office of Management and Budget, Paperwork Reduction Project (0704-0188), Washington, DC 20503.

1. AGENCY USE ONLY (*Leave blank*)	2. REPORT DATE	3. REPORT TYPE AND DATES COVERED
	July 1993	Technical Paper

4. TITLE AND SUBTITLE
Low-Current Traveling Wave Tube for Use in the Microwave Power Module

5. FUNDING NUMBERS
WU-506-72

6. AUTHOR(S)
Raymond W. Palmer, Peter Ramins, Dale A. Force, James A. Dayton,
Ben T. Ebihara, and Robert P. Gruber

7. PERFORMING ORGANIZATION NAME(S) AND ADDRESS(ES)
National Aeronautics and Space Administration
Lewis Research Center
Cleveland, Ohio 44135-3191

8. PERFORMING ORGANIZATION REPORT NUMBER
E-7329

9. SPONSORING/MONITORING AGENCY NAMES(S) AND ADDRESS(ES)
National Aeronautics and Space Administration
Washington, D.C. 20546-0001

10. SPONSORING/MONITORING AGENCY REPORT NUMBER
NASA TP-3344

11. SUPPLEMENTARY NOTES
Responsible person, Raymond W. Palmer, (216) 433-3518.

12a. DISTRIBUTION/AVAILABILITY STATEMENT
Unclassified - Unlimited
Subject Category 33

12b. DISTRIBUTION CODE

13. ABSTRACT (*Maximum 200 words*)

This report describes the results of a traveling-wave-tube/multistage-depressed-collector (TWT-MDC) design study in support of the Advanced Research Projects Agency/Department of Defense (ARPA/DOD) Microwave Power Module (MPM) Program. The study stressed the possible application of dynamic and other tapers to the rf output circuit of the MPM traveling wave tube as a means of increasing the rf and overall efficiencies and reducing the required beam current (perveance). The results indicate that a highly efficient, modified dynamic velocity taper (DVT) circuit can be designed for the broadband MPM application. The combination of reduced cathode current (lower perveance) and increased rf efficiency leads to (1) a substantially higher overall efficiency and reduction in the prime power to the MPM, and (2) substantially reduced levels of MDC and MPM heat dissipation, which simplify the cooling problems. However, the selected TWT circuit parameters need to be validated by cold test measurements on actual circuits.

14. SUBJECT TERMS	15. NUMBER OF PAGES
TWT; Microwave power; Module	16
	16. PRICE CODE: A03

17. SECURITY CLASSIFICATION OF REPORT	18. SECURITY CLASSIFICATION OF THIS PAGE	19. SECURITY CLASSIFICATION OF ABSTRACT	20. LIMITATION OF ABSTRACT
Unclassified	Unclassified	Unclassified	